Measurement of the Sintering Dynamics of polymeric powders at Near SLS Conditions

J. Steinberger, K. Manetsberger, J. Shen, J. Müllers

DaimlerChrysler Research Center
Ulm, Germany

Abstract

The sintering dynamics of materials used in the Selective Laser Sintering process impact greatly the thermal conditions of the powder bed. An experimental setup was developed to obtain sintering rate information at conditions very near to those of the SLS process. The system consists of a powder sample heated by a CO_2 laser while maintained at constant thermal boundary conditions. The powder height is measured by means of an optical sensor, which avoids stress on the powder and allows fast data acquisition. This paper discusses experiments conducted with this apparatus and further compares the obtained results with theoretical models and the previous work of others.

Introduction:

Selective laser sintering (SLS) can be seperated into three physical processes /NEL93/, /NÖK96/:

- Propagation of electromagnetic waves such as the laser and the heat radiation,
- Heat transfer in the powder bed, and
- Powder sintering due to thermal absorption of the laser power.

Sintering dynamics affect both the propagation of the laser radiation and thermal heat diffusion due to corresponding changes in powder bed porosity /Sch88/, /THI83/, /NEL93/. Since an understanding of sintering is important to modeling the SLS-process, a fair amount of theoretical and experimental work has been reported on this subject.

Sun /SUN91/ modeled sintering with an extension of the Frenkel model /FRE49/ by introducing an empirical sintering factor ξ, which described the probability of forming a neck between two adjacent particles. Weissman and Hsu /WEI91/ simulated the SLS process using Scherer's model for densification. Neither of these models were verified by experimental results. Nelson presented a simple phenomenological model dependent only upon rheological parameters of the material /NEL93/. He described densification according to the first order decay mechanism (Eq. (1)).

$$\frac{d\Psi}{dt} = -k \cdot (\Psi - \Psi_\infty) \tag{1}$$

where ψ is the solid fraction at time t, ψ_∞ is the solid fraction at $t = \infty$ and k is the sintering rate constant[1/s]. The sintering rate was described by an Arrhenius function:

$$k = A \cdot e^{-\frac{E_a}{R \cdot T}} \tag{2}$$

where A is the sintering coefficient [1/s], E_a is the activation energy [J/mol] and R is the gas constant [J/(molK)].

Sintering rate kinetics determined from isothermal, unidirectional powder densification studies as carried out by oven experiments were used to simulate SLS processing. While Nelson's empirical model showed reasonable agreement with his experimental results, the model fails to capture the true dynamics of the SLS process. Especially since, the empirical sintering rate of Eq. (1) was determined from data obtained at time scales several orders of magnitude larger then the time scales of the SLS process. Furthermore, the sintering rate was calculated by a change in powder sample height at constant temperature as determined by the aid of an applied stress. Lastly, the empirical sintering rate can not be inferred from physical material properties.

In this paper, a more suitable physical model is presented to describe the sintering dynamics of the SLS process. The model is then compared to an experiment, designed to be as close to the SLS process as possible.

Sintering Theory

German /GER96/ describes the viscous flow as the driving force for the sintering of polymers. Frenkel /FRE 45/ as corrected by Eshelby /ESH49/ first modeled sintering using viscous flow. Rosenzweig /ROS82/ verified the Frenkel model by studying the sintering of two PMMA spheres. Brink further demonstrated the Frenkel model to adequately describe the sintering of semicrystalline polymeric powders /BRI95/.

However, the Frenkel model is valid only for the initial sintering stage, since a change of the particle radius due to the sintering process is not considered. Pokluda modified the Frenkel model by considering the change in particle radius using the following equation /POK97/:

$$a(t) = a_0 \cdot \left(\frac{4}{(1 + \cos(\theta(t)))^2 \cdot (2 - \cos(\theta(t)))} \right)^{\frac{1}{3}} \tag{3}$$

where a(t) is the particle radius at time t and a_0 is the initial particle radius. The sintering angle θ is defined as

$$\frac{d\theta(t)}{dt} = \frac{\sigma}{\eta \cdot a_0} \cdot \frac{2^{-\frac{5}{3}} \cdot \cos(\theta) \cdot \sin(\theta) \cdot (2 - \cos(\theta))^{\frac{1}{3}}}{(1 - \cos(\theta)) \cdot (1 + \cos(\theta))^{\frac{1}{3}}} \tag{4}$$

$$\sin(\theta) = \frac{x}{a}$$

where σ is the surface tension, η is the viscosity and x is the radius of the sintering neck.

The Pokluda model describes the sintering of a two body system as the changing ratio of the sintering neck x to the particle radius a. This quantity must be used to describe densification or the change in solid fraction, ψ, in the SLS process. *Figure [1]* shows a characteristic volume element of the powder used to determine the solid fraction as a function of the sintering neck. It consists of a cylindrical unit cell containing two half-particles surrounded by an airjacket. This airjacket is used to explain the difference between the calculated solid fraction of the cell ψ_{unit} and the experimentally measured solid fraction. The solid fraction of the unit cell can be calculated as:

$$\psi_{unitcell} = \frac{V_{neck} + V_{residual\_sphere}}{V_{cylinder}} \tag{5}$$

$$\psi_{unitcell} = x^2 + \frac{2}{3} \cdot (1 - x^2)^{\frac{3}{2}}$$

The volume of the airjacket is such that $\psi_{theoretical}$ and $\psi_{experimental}$ are equal for $t = 0$.

$$\Psi(t = 0)_{theoretical} = \Psi(t = 0)_{control\_volume} = \frac{V_{solid}}{V_{control\_volume}} = \frac{V_{solid}}{V_{unit\_cell} + V(t = 0)_{airjacket}} \tag{6}$$

If the control volume is scaled to 1, the volume of the airjacket at $t = 0$ is given by

$$V(t = 0)_{airjacket} = 1 - \frac{\Psi_{experimentally}}{\Psi(t = 0)_{unit\_cell}} \tag{7}$$

As the neck grows, the volume of the airjacket must decrease. By assumig the decline of the airjacket being proportional to the growth of the solid fraction in the unit cell, the volume of the airjacked at time t is given by

$$V_{airjacket} = (1 - \frac{\Psi_{experimentally}}{\Psi(t = 0)_{unitcell}}) \cdot \frac{1 - \Psi_{unitcell}}{1 - \Psi(t = 0)_{unitcell}} \tag{8}$$

Therefore, the solid fraction of the control volume becomes

$$\Psi = \Psi_{unitcell} \cdot (1 - V_{airjacket})$$

$$\Psi = \left(x^2 + \frac{2}{3} \cdot (1 - x^2)^{\frac{3}{2}} \right) \cdot \left(\left(\frac{\Psi_{experimentally}}{\frac{2}{3}} \right) \cdot \frac{1 - x^2 - \frac{2}{3} \cdot (1 - x^2)^{\frac{3}{2}}}{1 - \frac{2}{3}} \right) \tag{9}$$

Eq. (9) is material independent, so it can be compared with experimental data for any material. *Figure [2]* shows the comparison to experimental data for glass /GER96/.
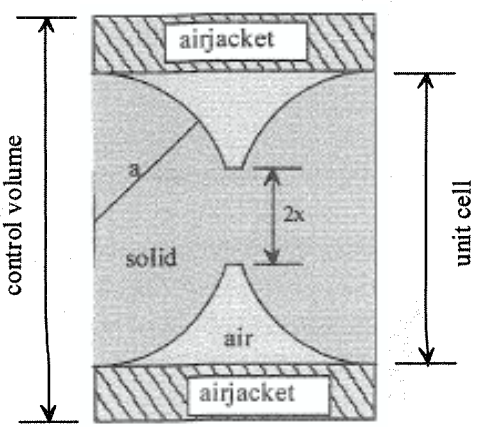
Figure[1]: *Characteristical volume element*
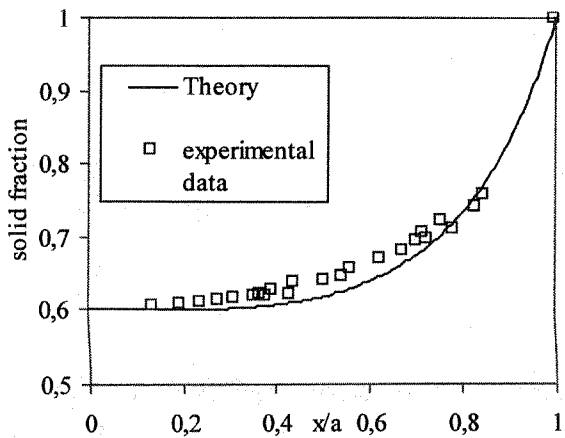
Figure [2]: *Comparison of Eq. (9) and experimental data for glass*

Experimental analysis of the sintering dynamics

Experimental setup: *Figure [3]* shows the experimental apparatus used to measure powder sintering dynamics. Powder is placed on a heating stage and preheated to the desired temperature. The powder is then exposed to CO_2 laser radiation (Synrad-laser, 10W). An optical sensor (Jurca Optoelektronik) is used to follow the change in sample height. The sensor uses the spherical abberation of a lens and therefore volume effects can be neglected. It has a focal spot of 10 μm, an accuracy of 0.1 μm, and a sampling rate of up to 1000 Hz. The working distance is 5 mm thus the laser beam had to be focused by an optical system on the powder bed under an angle δ of 13.5°.
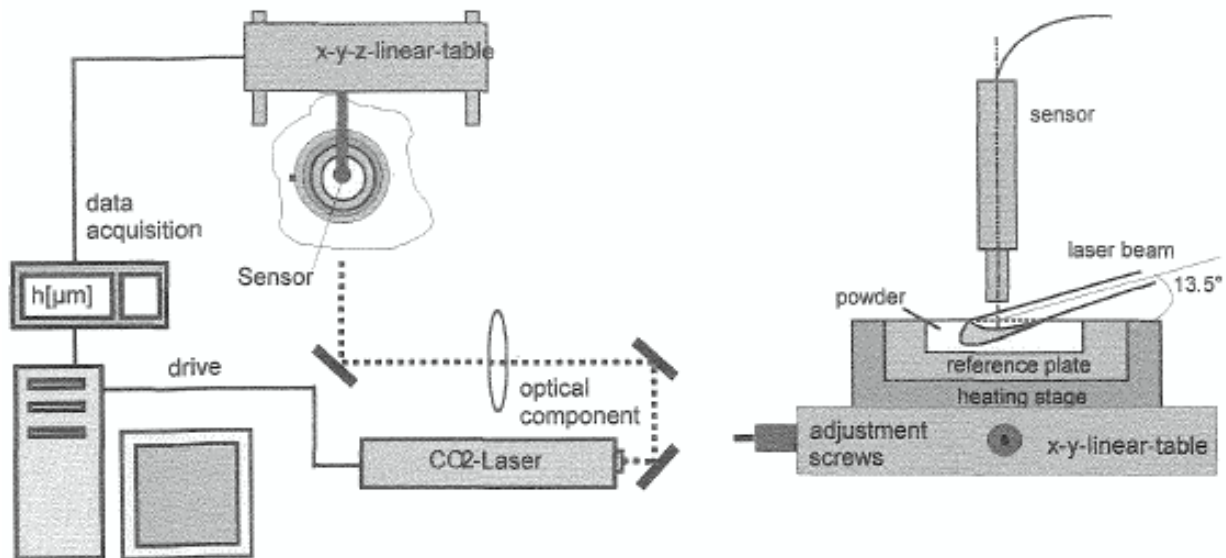
Figure [3]: experimental setup

Experimental procedure: The applied laser energy density during the experiment corresponded to values used in the SLS-process. It was changed by varying both the laserpower and the exposure time. The spot size was enlarged to 4.25 mm to minimize border effects. Thus, homogeneous conditions within the measuring spot can be assumed. To compare experimental data with theoretical predictions, the temperature in the laser spot was also measured. Variations in the applied energy density due to the 13.5° working angle were corrected by an appropriate coordinate transformation.

Since the working angle was limited to 30°, small lateral movements of the measured powder sample could lead to a loss of the sensor signal. Therefore, a series of measurements for PMMA as well as for PA were averaged for each condition. Curves represented in this paper are the result of at least seven independent measurements for each condition.

Experimental results (PMMA): *Figure [4]* shows the change in powder height, dh, for different laser energies for a characterized PMMA. The PMMA powder partical have a spherical shape and an average radius of 16.5 μm. The laser energy was applied to the powder bed 5 s after the measurement was started. Immediately the powder began to expand.
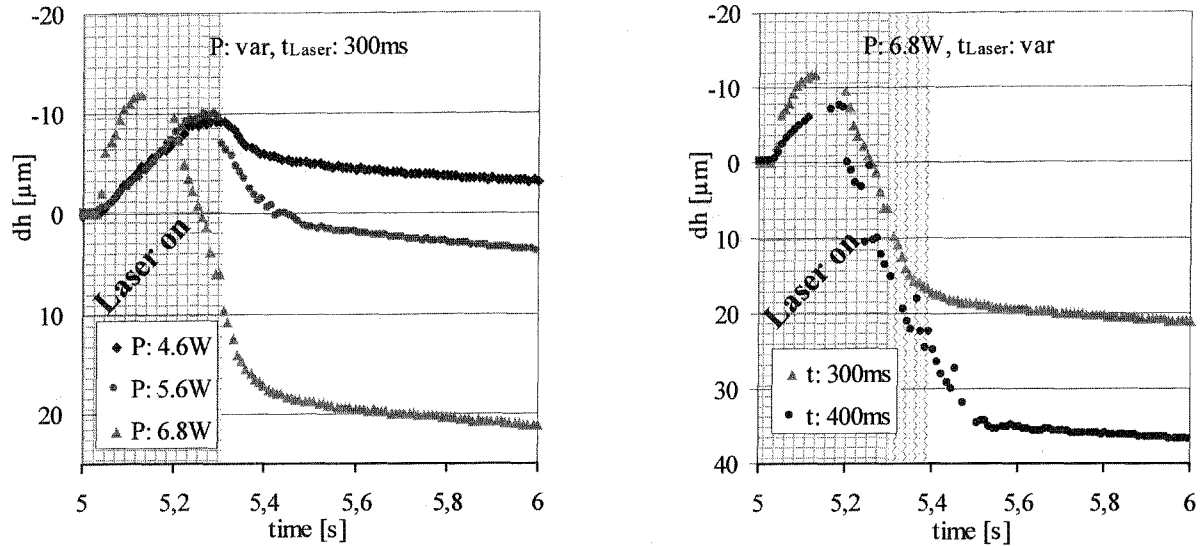
Figure [4]: change of heigth of a sintered PMMA-powder

Nelson also observed a similar expansion in his experiments and reasoned it was due to a change of particle geometry from ellipsoidal to spherical. In the present work, however, PMMA is spherical. *Figure [5]* compares the thermal expansion, dl, of PMMA powder to solid PMMA. In order to compare the expansion curves of the powder and the solid, the rate of thermal expansion is estimated by:

$$\Delta l = \alpha \cdot \Delta T \cdot D_p = \alpha \cdot \frac{P \cdot \Delta t \cdot r \cdot \cos(90 - \delta)}{\frac{\pi}{2} \cdot a_0 \cdot b_0 \cdot D_p \cdot \varphi \cdot \Psi_{exp} \cdot c_p} \cdot D_p$$

$$\left(\frac{\Delta l}{\Delta t}\right)_{solid} = \frac{P_{solid}}{P_{powder}} \cdot \Psi_{exp} \cdot \left(\frac{\Delta l}{\Delta t}\right)_{powder}$$

$$\left(\frac{\Delta l}{\Delta t}\right)_{solid} = 1.93 \cdot \left(\frac{\Delta l}{\Delta t}\right)_{powder} \quad \text{for } P_{solid} = 6,8W \text{ and } P_{powder} = 1,9W$$

(10)

where D_p is the penetration depth of the laser beam, r is the absorbed fraction of the laser beam, a_0 and b_0 are the semiaxis of the elliptical laser beam, φ is the density of the solid material and c_p is the specifical thermal capacity.

Comparing Eq. 10 to the experimental data in *Figure [5]* for $\Delta t = 150ms$, the effective thermal expansion of the powder is about 2,5 times higher than the theoretical thermal expansion. We think, this due to a possible expansion of the gas.

As the laser power is increased with constant exposure time, the sintering rate is enhanced. Moreover the onset of sintering t_{start} is decreased to shorter times. The activation energy, E_a, necessary to start the sintering process is achieved more rapidly using the higher laser power. Changing the applied energy by varying the exposure time with constant laser does not change either the sintering rate or the starting point of the sintering process. However, *Figure [6]* shows that the absolute change in height, dH, the change of height for t = ∞, and therefore the absolute change in solid fraction does change.
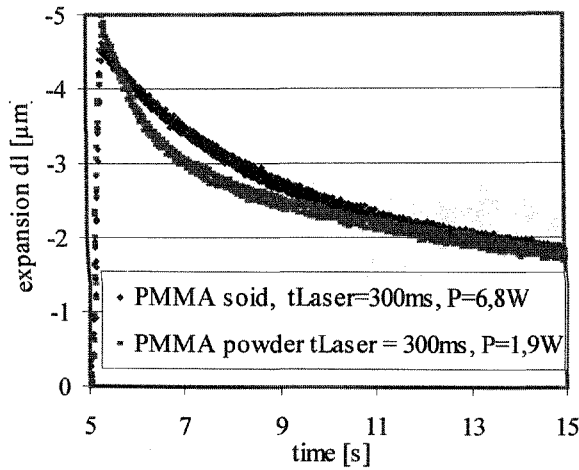
Figure [5]: Comparison of the expansion curves of solid and powder (PMMA)
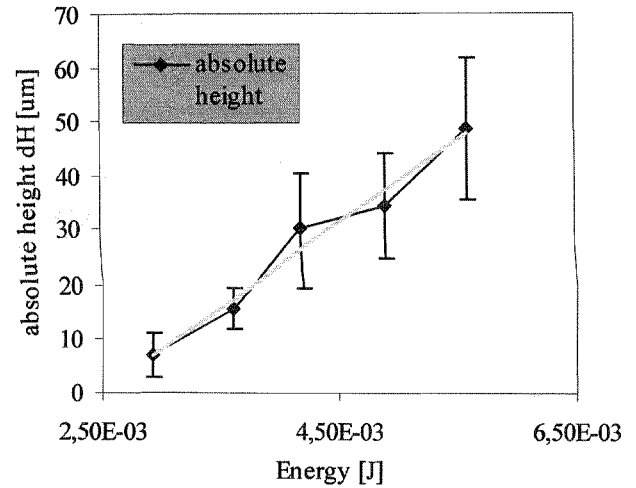
Figure [6]: Cbsolute change in height dH

Depending on the laser power, the sintering starts after 200ms. For the heat conduction and the propagation of electromagnetic waves, however, only the densification due to the sintering is relevant. Therefore, the thermal expansion was measured and then substracted from the measured values as shown in *Figure [4]*. The result is shown in *Figure [7]*.
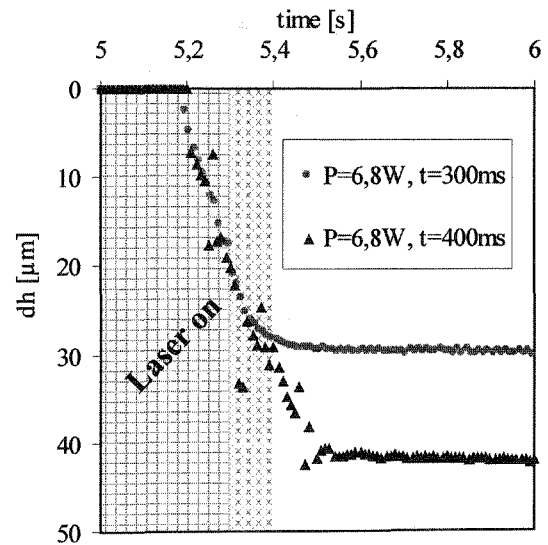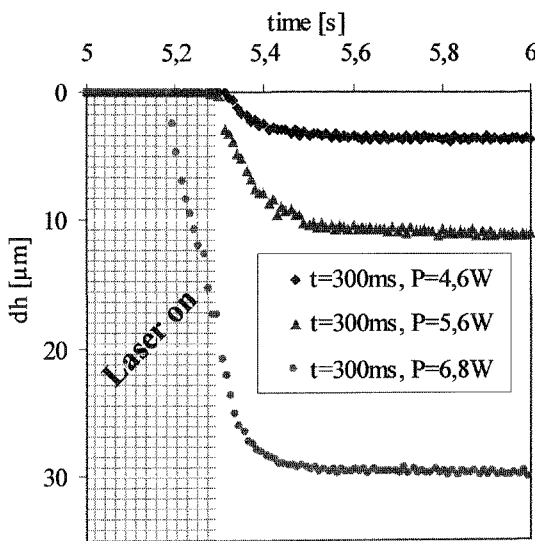
Figure [7]: Scaled sinter dynamics (PMMA)

Evaluation of the sintering theory

To compare theoretical and experimental results, the temperature at the laser spot was measured during the sintering process. The results are shown in *Figure [8]*. Since a temperature gradient exists in the heated spot, it follows that only an average change of solid fraction can be measured. To judge one model properly, the experiment needs to be simulated by taking the temperature distribution into account. This is our research of immediate interest. For a rough estimation, however, the solid fraction at t = ∞ in the experiments is compared to the solid fraction at t = ∞ for parts, build at the same energy densities as in the "real" SLS.

308
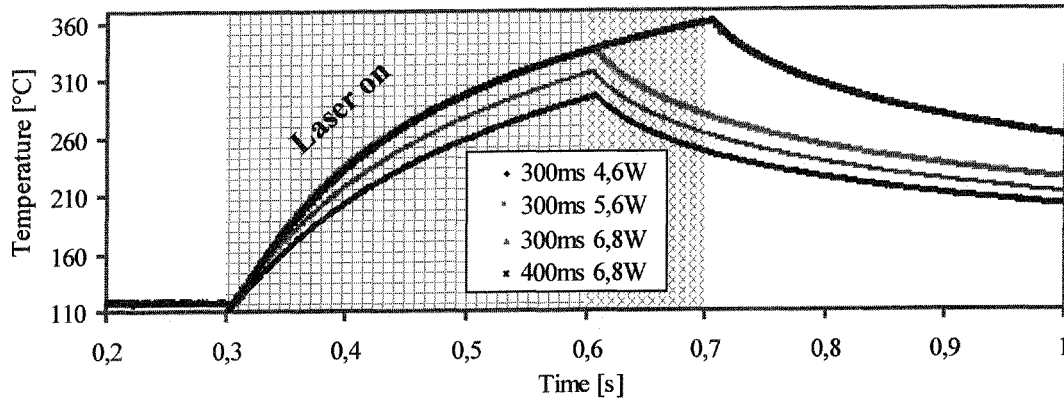
Figure [8]: Temperature in the laserspot (PMMA)

Data for Nelson's empirical model were obtained for the PMMA material used in this study to provide a comparison between the two models. The sintering rate was determined to be:

$$k = 4.15 \cdot 10^5 \cdot e^{-\frac{79.451 \cdot 10^3}{R} \frac{1}{T}} \cdot \frac{1}{s}$$

Discussion: *Figure [9]* shows model results compared to a set of experimental data (400ms, 6,8W). The necessary physical properties were either determined experimentally or taken out from the literature. Clearly, Nelson's model does not adequately describe the sintering dynamics. The modified Pokluda model, describes sintering dynamics better, but kinetics are still too slow, especially since temperature gradients in the powder are not taken into account.
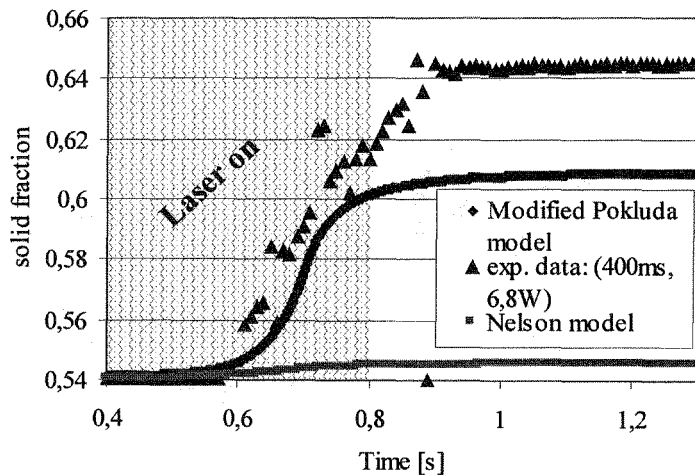
Parameters:

$$\eta = 1.95 \cdot 10^{-8} \cdot e^{\frac{1.241 \cdot 10^5}{8.3123 \cdot T}} [Pa \cdot s]$$

$a_0 = 15 \mu m$

$\sigma = 25 \cdot 10^{-3} \frac{N}{m} (/ROS81/)$

$\Psi_{exp} = \Psi_0 = 0.54$

$\Psi_\infty = 1$

$P_{Laser} = 6.8W$

$t_{Laser} = 400ms$

Figure [9]: Comparing the modified Pokluda model and the Nelson model to experimental data

Sintering dynamics of Nylon:

The melting dynamics of PA-12 for the experimental conditions (300ms, 3,3W) are of the same time scale as for the sintering dynamics of PMMA (*Figure [10]*). The absolute change of the solid fraction, however, is higher, since PA-12 is a semi-crystalline material.
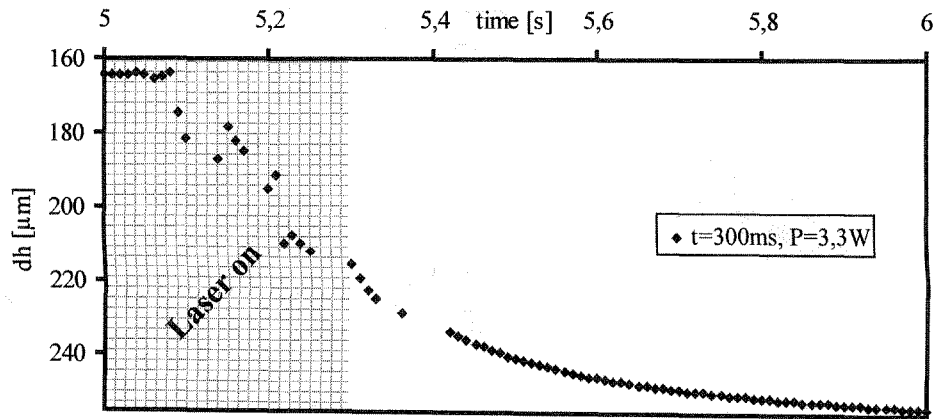
Figure [10]: *sintering dynamics of PA-12*

Conclusions

Unlike to other experiments, the sintering dynamics were measured at near SLS conditions. This was achieved using instantaneous heating with a laser and by data acquisition with a fast optical sensor. The results show that the modified Pokluda models describes the dynamics of the SLS process better than the Nelson model. It appears, that this modell could be improved and adapted to the SLS process. One possible improvement could be the consideration of viscoelastic effects /BEL98/, /MAZ94/. However further information can only be obtained by simulating the experiment.

Acknowlegement

The autors kindly thank Dr. Neal K. Vail for his input on this work

References

C. T. Bellehummeur /BEL98/: *The role of viscoelasticity in polymer sintering* Rheol Acta 37: 270 – 278 (1998)	**S. Nöken /NÖK97/:** *Technologie des Selektiven Lasersinterns von Thermoplasten, Diss* Shaker Verlag, Band 8, 1997
A. E. Brink /BRI94/: *Sintering high performance semicrystalline polymeric powders* Polymer Eng. And Science, Dec. 95, Vol. 35, No. 24	**O. Pokluda /POK97/:** *Modification of Frenkel's model for sintering* AIChE Journal, Dec97, Vol. 43, No. 12
J. D. Eshelby /ESH49/: *Seminar on the kinetics of sintering* Metals transaction 185 (1949), S 806 - 807	**N. Rosenzweig /ROS81/:** *Sintering Rheology of Amorphous Polymers* Polymer Eng. And Science, Dec. 81, Vol. 21, No. 17
J. Frenkel /FRE45/ *Viscous flow of crystalline bodies under the action of surface tension* *Journal of Physics, 1945, Vol IX, No. 5*	**E. U. Schlünder /SCH88/:** *Wärmeübertragung in Festbetten, Schüttgütern und Wirbelschichten* Georg Thieme Verlag Stuttgart, 1988
R. M. German /GER96/: *Sintering theory and practice* John Wiley & Sons, Inc. New York 1996	**M. Sun /SUN91/:** *A Model for Partial Viscous Sintering* Solid Freeform Fabrication Symposium 1991
S. Mazur /MAZ94/: *Viscoelastic effects in the coalescence of polymer particles* Progress in organic coatings 24 (1994) 225 - 236	**C. L. Tien /TIE87/:** *Thermal Radiation in Particulate Media with Dependent and Independent Scattering* Annual Review of Numerical Fluid Mechanics and Heat Transfer, 1, pp. 1-32, 1987
J. C. Nelson /NEL93/: *Selective Laser Sintering: A Definiton of the Process and Empirical Sintering Model*; PhD, Dissertation , 1993; Univ. of Texas	**E. M. Weissman /WEI91/:** *A Finite Element Model of Multi-Layered Laser Sintering Parts* Solid Freeform Fabrication Symposium 1991